Polyamines regulate cell fate by altering the activity of histone-modifying enzymes.

Maya Emmons-Bell[1], Grace Forsyth[2,*], Abby Sundquist[1,*], Sylvie Oldeman[3], Angeliki Gardikioti[1], Roshni de Souza[1], Jonathan Coene[4], Maryam H. Kamel[5], Shine Ayyapan[6], Harrison A. Fuchs[6], Steven Verhelst[4], Joanna Smeeton[5], Catherine A. Musselman[6], Juan-Manuel Schvartzman[1,7,8]

[1]Columbia University, Herbert Irving Comprehensive Cancer Center, New York, NY, USA; [2]Weill Cornell Medical College, New York, NY, USA; [3]Barnard College, New York, NY, USA; [4]University of Leuven, Cellular and Molecular Medicine, Leuven, Belgium; [5]Columbia Stem Cell Initiative, Department of Rehabilitation and Regenerative Medicine, and Department of Genetics and Development, Columbia University Irving Medical Center, Columbia University, New York, NY, USA; [6]Department of Biochemistry and Molecular Genetics, University of Colorado Anschutz Medical Campus, Aurora, CO, USA; [7]Columbia University Irving Medical Center, Department of Medicine, Division of Hematology/Oncology, New York, NY, USA.

[8] Corresponding author

* These authors contributed equally.

Abstract

Polyamines are polycationic alkyl-amines abundant in proliferating stem and cancer cells. How these metabolites influence numerous cellular functions remains unclear. Here we show that polyamine levels decrease during differentiation and that inhibiting polyamine synthesis leads to a differentiated-like cell state. Polyamines concentrate in the nucleus and are further enriched in the nucleoli of cells in culture and *in vivo*. Loss of polyamines drives changes in chromatin accessibility that correlate with altered histone post-translational modifications. Polyamines interact electrostatically with DNA on the nucleosome core, stabilizing histone tails in conformations accessible to modifying enzymes. These data reveal a mechanism by which an abundant metabolite influences chromatin structure and function in a non-sequence specific manner, facilitating chromatin remodeling during reprogramming and limiting it during fate commitment.

Introduction

The polyamines putrescine, spermidine and spermine are polycationic (positively-charged) alkyl-amines present at high concentrations in eukaryotic cells (*1*, *2*). Polyamines are synthesized by decarboxylation of the amino acid ornithine by the enzyme ornithine decarboxylase (ODC1) (Fig. 1A). At approximately 1 mM, polyamine concentration in proliferating cells is within the range of abundant amino acids like glutamine (*2*, *3*). Polyamine biosynthesis is upregulated in proliferating cells, while its inhibition results in cell cycle arrest (*4–6*). In some cases, this arrest resembles terminal differentiation (*7–9*). Consistent with proliferating cells requiring high levels of polyamines, ODC1 is a top transcriptional target of the transcription factor MYC(*10*), and upregulation of ODC1 is required for the transforming effects of MYC(*11*, *12*). ODC1 is an irreversible enzyme in metazoans, therefore cells cannot recover carbon or nitrogen from existing polyamine pools. Thus, proliferating cells invest a significant fraction of critical nutrients (e.g. glutamine and arginine) in the irreversible production of polyamines, yet their biological role is poorly understood.

Mechanistically, polyamines have been shown to perform multiple biological functions, including participating in the post-translational modification of the translation initiation factor eIF5A (*13*, *14*) and regulation of inwardly rectifying potassium channels (*15*). Earlier work has also shown that polyamines interact with negatively-charged macromolecules like DNA and RNA. This interaction with DNA can alter chromatin accessibility and increase transcriptional efficiency *in vitro* (*16–19*), but whether and how this occurs *in vivo* is unknown. Here we show that polyamines are enriched in the nucleus, where their interaction with chromatin enables increased accessibility of the histone tail to chromatin modifying enzymes. These interactions are critical for the regulation of cell state. By decreasing polyamine levels, differentiating cells limit noisy chromatin dynamics, enabling faithful lineage commitment. Conversely, increasing intracellular polyamine concentrations facilitates lineage plasticity and reprogramming. Thus, polyamines alter the flexibility of chromatin landscapes in an enzyme- and sequence-agnostic manner, facilitating a broad diversity of cell state transitions.

Results

Polyamine biosynthesis is decreased during differentiation.

Since polyamine content is highest in undifferentiated cells, we wondered if polyamine metabolism is regulated during differentiation. To explore transcriptional regulation of polyamine biosynthesis, we mined published RNAseq datasets in diverse models of differentiation. Across many models (3T3L1 cells during adipocyte differentiation, 10T1/2 cells during osteoblast differentiation, human chondrocyte tissue sam-

ples during early development, human embryonic stem cells during neuronal differentiation, C2C12 cells during myotube differentiation, and human hematopoietic cells), we found that ornithine decarboxylase (ODC1) expression decreased as cells underwent fate commitment (Fig. 1B). Expression of spermidine synthase similarly decreased over differentiation, however spermine synthase expression was not clearly correlated with differentiation state in every model (Fig. S1A-D). We next asked if cellular polyamine content similarly decreased as cells differentiated. We used two well established progenitor models, pluripotent murine mesenchymal progenitors (10T1/2 cells), which we differentiated into chondrocytes, and murine myoblasts (C2C12 cells), which we differentiated into myotubes. We validated induction of differentiation by western blot for lineage markers (Fig. 1C). To quantify cellular polyamine content, we optimized a protocol for polyamine extraction and derivatization for gas chromatography mass spectrometry (GC-MS) (See Materials and Methods)(*20*). In both models, we found that levels of putrescine decreased by 40-50% after twenty-four hours in differentiation media (Fig. 1D and E) and remained low as cells continued differentiating. In 10T1/2 cells, the levels of spermidine increased slightly at days five and seven of differentiation (Fig. 1D), but spermine levels decreased as cells committed to a chondrocyte fate (Fig. 1D). In C2C12 cells undergoing myotube differentiation, spermidine and spermine levels decreased twofold after twenty-four hours in differentiation media (Fig. 1E). We next mined a published metabolomics data set collected over the first ninety-six hours of zebrafish development and found that putrescine and spermidine levels increased for 48h after fertilization, but then decreased as cells began to differentiate (Fig. S1E and Fig. S1F; N.B. spermine abundance was not reported). These data demonstrate that across multiple models and at both the transcriptional and metabolite-levels, polyamine levels decrease during lineage commitment.

Polyamine depletion induces a differentiated-like cell state.

We next asked if polyamine depletion might play a causative role during differentiation. To test this, we depleted cells of polyamines and assessed their differentiation states. We used CRISPR-Cas9 to genetically ablate ODC1 in 10T1/2 cells (Fig. S2A), and validated the effect of ODC1 knockout on polyamine content with GC-MS. The abundances of all three polyamine species were decreased in knockout cells (Fig. 2B, Fig. S2B). We also targeted ODC1 pharmacologically by treating cells with the irreversible ODC1 inhibitor difluoromethylornithine (DFMO), which decreased the abundance of all three polyamine species to a similar extent as ODC1 knockout (Fig. S2C).

Polyamines are known to be required for cell proliferation (*4*, *21*). Consistent with this, DFMO-treated and ODC1 knockout cells failed to proliferate following three days of polyamine depletion (Fig. 2A). We did

not observe decreases in cell number or viability (Fig. S2D) which would indicate widespread cell death, suggesting that the effect of polyamine depletion is cytostatic. EdU incorporation and cell cycle analysis by flow cytometry showed that polyamine depleted cells were specifically arrested in G1 (Fig. S2E). We were able to rescue the cytostatic effect of polyamine depletion in ODC1 knockout cells by supplementing media with 0.5 mM putrescine, validating enzymatic loss of function and indicating that knockout cells behaved like putrescine auxotrophs (Fig. 2A).

To our surprise, polyamine depletion resulted in changes in morphology in 10T1/2 cells. While wild-type 10T1/2 cells are normally cuboidal in shape, ODC1 knockout and DFMO-treated cells became elongated and spindly (Fig. 2C). The combination of cell cycle arrest in G1 and changes in morphology suggested that polyamine-depleted cells might be undergoing a differentiation-like change in cell state. To explore whether polyamine depletion was leading to differentiation, we carried out RNAseq on control and ODC1 knockout cells treated with DFMO or exogenous putrescine, grouped the cells according to low or high polyamine content as assessed by GC-MS, and performed differential gene expression analysis (Fig. 2D). Genes upregulated in polyamine-depleted samples were involved in the regulation of diverse cell differentiation outcomes, multicellular development, and intracellular signal transduction (Fig. 2E, top terms shown in Fig. S2F). Conversely, gene sets down-regulated in polyamine-depleted cells were involved in cell cycle regulation (Fig. 2E, top terms shown in Fig. S2G), agreeing with the cytostatic effect of polyamine depletion. Critically, polyamine depletion did not lead to upregulation of genes associated with any one lineage, suggesting that polyamine depletion is not inducing differentiation on its own, but rather promoting a “differentiation-like” or “differentiation-primed” cell state.

A hallmark of terminal differentiation is irreversible exit from the cell cycle. To explore whether the arrest in G1 observed in polyamine-depleted cells was reversible, we treated cells with DFMO for three days, then allowed them to recover for three days in media without drug. Polyamine-depleted cells did not resume proliferation after drug washout (Fig. 2F). Thus, DFMO treatment induces an irreversible exit from the cell cycle. Taken together, these data suggest that polyamine depletion pushes cells towards a more differentiated phenotype.

To test whether polyamine depletion induces differentiation in other contexts, we treated a panel of cell lines with DFMO and assessed expression of lineage commitment markers by western blot. In 10T1/2 cells cultured in chondrocyte differentiation media, DFMO treatment either 24 hours before or at the onset of differentiation increased differentiation marker expression (Fig. 2G). However, DFMO had a negative

effect on differentiation if present once the differentiation process was underway. We saw similar behavior in C2C12 myoblasts induced to differentiate into myotubes; DFMO treatment during the myoblast stage was able to prime differentiation, but impaired differentiation if added during the final stages (Fig. 2G). As opposed to these non-transformed models of differentiation, in three cancer cell lines tested (SK-N-BE(2) neuroblastoma, COLO858 melanoma, and Ki562 acute myeloid leukemia) polyamine depletion resulted in decreased proliferation (Fig. S3A) and up-regulation of markers of differentiation (Fig. 2G). Thus, when polyamines are depleted, non-transformed progenitors are primed for increased differentiation while transformed cells are pushed towards a differentiation-like state.

Polyamines are known to contribute to translational homeostasis through spermidine's role as a substrate for eIF5a hypusination (*13*, *14*). Hypusinated eIF5a facilitates the translation elongation and termination of polyproline-rich and tripeptide repeat-containing proteins (*22–24*), and it has been suggested that polyamines impact growth and lineage fidelity through their regulation of hypusination (*25*). To investigate whether polyamine-depleted 10T1/2 cells were undergoing proteotoxic stress, we pulsed cells with the puromycin analogue O-propargyl-puromycin (OPP) and quantified global translation by flow cytometry. We did not observe changes in bulk translation following depletion or addition of polyamines (Fig. S3B, C), nor did we observe induction of phosphorylated eIF2a, a readout of the integrated stress response (Fig. S3D)(*26*). To explore the impact of hypusination on differentiation, we pharmacologically inhibited deoxyhypusine synthase (DHPS), the enzyme responsible for forming the first intermediate deoxyhypusine residue on eIF5a. We validated decreased hypusine levels following DHPS inhibition by western blot. Markers of differentiation either decreased or did not change (Fig. S3E) after DHPS inhibition. These data suggest that the differentiation phenotypes observed after polyamine depletion are not due to impaired hypusination.

Polyamines are localized in nuclear and sub-nuclear compartments.

Subcellular compartmentalization of metabolites can target the effects of metabolism to specific parts of a cell, even in the absence of membrane-bound organelles (*24*). We reasoned that identifying where polyamines were concentrated in cells might help illuminate their mechanism of action. Resolving subcellular localization of metabolites by mass spectrometry is currently limited by the spatial resolution of MALDI (Matrix-Assisted Laser Desorption/Ionization) (*25*, *26*), so we set out to identify an alternative imaging-based approach. We synthesized a clickable putrescine probe consisting of putrescine with an azide group that can be covalently bound to a fluorophore-alkyne label *in vitro* or *in vivo* (Fig. 3A). We treated live cells with the un-clicked probe, fixed, permeabilized and performed click-chemistry to a fluorophore alkyne, and then imaged cells using confocal microscopy. We did not observe any fluorescence signal

when cells were exposed to the probe without an alkyne fluorophore (Fig. S4A). Imaging after clicking the probe to a fluorophore revealed stark nuclear localization in 10T1/2 cells (Fig. 3B). We also observed sub-nuclear regions of probe localization, which corresponded with localization of NPM1, a protein component of the nucleolus (Fig. 3C and Fig. 3D). Nuclear and nucleolar probe localization was also observed in C2C12 and U-2 OS cells (Fig. S4C and Fig. S4D). To determine if polyamines are primarily associated with chromatin (DNA and protein), or RNA species, we incubated cells in the putrescine probe, and then treated cells with RNAse. Following RNAse treatment, cells were washed thoroughly and imaged. Nuclear and nucleolar probe localization was observed regardless of RNAse treatment (Fig. 3E and Fig. S4E), suggesting that polyamines are primarily associated with chromatin in the nucleus. To validate our localization data *in vivo*, we manually dechorionated zebrafish embryos at the four-cell stage and exposed them to the putrescine probe for two hours, then fixed, permeabilized, and performed click chemistry. In this case, the putrescine probe was concentrated in nuclei, especially at the nuclear periphery (Fig. S4F). At this stage of development (roughly four hours post fertilization), nucleoli have not yet formed, thus explaining the lack of nucleolar enrichment (*21*). We next incubated and imaged cells with spermidine and spermine probes and found that these were also enriched in the nucleus and nucleolus (Fig. 3F and Fig. S4B). Taken together, our data suggest that all three polyamine species concentrate in the nuclei of cells *in vitro* and *in vivo*, where they primarily associate with chromatin.

Polyamines regulate chromatin accessibility by increasing the activity of diverse histone modifying enzymes.

Polyamines have been reported to alter DNA/DNA and DNA/protein interactions (*27*, *28*). Given their nuclear localization and the effects of polyamine depletion on differentiation, we set out to explore the impact of polyamine depletion on chromatin. We first profiled chromatin accessibility broadly by performing micrococcal nuclease (MNase) digestions on wildtype and ODC1 knockout 10T1/2 cells and quantifying the abundance of mononucleosome fragments. Mononucleosome abundance was increased in ODC1 knockout cells (Fig. S5A), suggesting that global chromatin accessibility increases upon polyamine depletion. To determine the specificity of this change in chromatin accessibility, we performed ATACseq (Assay for Transposase-Accessible Chromatin using sequencing) on 10T1/2 cells treated with DFMO or putrescine (Fig. 4A and Fig. S5B). Addition of putrescine had minimal effects on chromatin accessibility, but polyamine depletion resulted in thousands of regions of chromatin with either increased or decreased accessibility (Fig. 4A, Sup. Fig. 5C, samples normalized to E. coli spike-in DNA). As we had seen with MNAse treatment, and consistent with earlier reports(*19*), we noticed an overall increase in chromatin accessibility in DFMO-treated samples. At a more granular level, genes with increased accessibility in transcriptional

start sites following polyamine depletion were associated with the regulation of anatomical structure size, morphogenesis, and cell adhesion (Fig. S5D), and *de novo* motif enrichment analysis revealed binding sites for transcription factors known to coordinate lineage and responses to diverse stressors (Fig. S5E). Together with our transcriptomic data, these results suggest that polyamine depletion initiates a concerted rewiring of epigenetic and transcriptional landscapes, pushing cells towards a more differentiated state.

Changes in chromatin accessibility are coordinated in part by enzymes that deposit modifications on histone tails. To characterize histone tail modifications following polyamine depletion, we assessed the levels of a panel of histone modifications by western blot, finding that some modifications increased, some decreased, and some were unaltered (Fig. S5F). These changes were not due to the cytostatic effects of polyamine depletion, as arresting cells in G1 with palbociclib did not induce changes in H3K18ac or H3K9me2 (Fig. S5G). Additionally, we did not observe changes in global DNA 5mC content (Fig. S5H). We next wanted to understand how polyamine depletion might alter histone tail modifications. A challenge of interpreting changes to bulk histone modifications is that they are the sum of the activities of both writer and eraser enzymes. Therefore, we set out tease apart the effect of polyamine depletion on classes of histone modifying enzymes. We exposed 10T1/2 and SK-N-BE(2) cells to inhibitors of histone acetyltransferases (JG2016, HATi) or histone deacetylases (Vorinostat, HDACi) and depleted polyamines with DFMO. We reasoned that DFMO treatment in the context of histone writer inhibition (HATi) would allow us to assess the impact of polyamine depletion on histone eraser activity, and vice versa. HATi treatment decreased histone acetylation, reflecting the accumulated activity of deacetylases (Fig. 4B). Polyamine depletion in the presence of histone acetyltransferase inhibition attenuated this decrease (Fig. 4B), suggesting that polyamine depletion decreases the activity of histone deacetylase enzymes. The same effect was seen after inhibition of deacetylases – increased acetylation following HDACi treatment was decreased by concomitant polyamine depletion (Fig. 4B) – as well as methyltransferase and demethylase inhibition, to varying extents in the two cell lines tested (non-transformed 10T1/2 cells and transformed SK-NE-B(2) cells) (Fig. S5I). This data led us to conclude that polyamine depletion can decrease the activity of diverse classes of histone-modifying enzymes.

We next hypothesized that increased polyamine concentrations might facilitate histone modification reactions. To directly query the impact of polyamines on histone modifying enzymes, we performed *in vitro* histone modification reactions with purified enzymes, cognate substrates, recombinant nucleosomes, and polyamines. The addition of putrescine increased the efficiency of H3K9me2 demethylation by KDM4A (Fig. 4C), in agreement with our *in vivo* results. We observed the same effect when KDM4A was

incubated with spermine (Fig. S5J). We performed equivalent *in vitro* histone deacetylation (Sirt6), acetylation (GCN5), and methylation (G9a) reactions, and found in each case at least one polyamine species increased enzymatic activity (Fig. 4D-F). These data suggest that polyamine species increase the catalytic activity of multiple subclasses of histone-modifying enzymes.

Deuterium exchange mass spectrometry data has shown that histone tails are solvent protected, likely due to their electrostatic interactions with the DNA backbone (*29*). To serve as substrates of enzymatic activity, polycationic histone tails must dissociate from negatively charged nucleosomal gyre DNA. We hypothesized that this dissociation was favored by polyamines, which would bind electrostatically to the DNA backbone and allow the histone tail to become freely available to diverse classes of histone modifying enzymes. To test the requirement for DNA/histone interactions on enzymatic sensitivity to polyamines, we performed *in vitro* acetylation experiments using bulk histone protein as a substrate. We found no changes in histone acetylation upon polyamine addition in this setting (Fig. 4G). Another prediction of this model is that as opposed to modifications of the relatively unstructured histone tail, modifications to the core histone particle, like histone H3K79 di-methylation catalyzed by the enzyme DOT1L, would not be impacted by polyamines. To test this, we treated 10T1/2 cells with DFMO alone or in combination with EPZ5676, an inhibitor of DOT1L(*30*), and found that H3K79me2 levels were unchanged (Fig. S5K). We next performed *in vitro* histone methylation reactions with recombinant DOT1L protein and found that enzymatic activity was unaffected by addition of polyamines (Fig. 4H). Importantly, we did not find evidence that polyamines at the concentrations used in our *in vitro* assays could denature DNA from the nucleosome core (Fig. S5L)(*31*).

To further characterize how polyamines affect histone tail conformation, we performed nuclear magnetic resonance (NMR) experiments. Previous studies have supported that H3 tails are associated with DNA in the context of nucleosomes, forming a fuzzy complex that can be regulated by histone post-translational modifications and nucleosome composition (*32–36*). To test if spermidine can alter the conformation and accessibility of the H3 tail, we carried out chemical shift perturbation (CSP) experiments on the nucleosome core particle (NCP) in which H3 was ^{15}N-labelled (^{15}N-H3-NCP). With this labeling scheme, H3 tails are observable within the context of the nucleosome. We collected ^{1}H,^{15}N heteronuclear single quantum coherence (^{1}H,^{15}N-HSQC) spectra on the ^{15}N-H3-NCP in the absence and presence of spermidine (Fig. 4I-J and Fig. S5M-O). In the presence of spermidine we observed CSPs consistent with altered H3 tail conformational ensemble. These CSPs were observable across the entire H3 tail, indicating that all residues are affected by spermidine. The direction of the CSPs are consistent with previously observed CSPs

seen with addition of increasing monovalent or divalent salt concentrations (*33*) which are known to enhance the accessibility of the H3 tail. These *in vitro* experiments suggest that polyamines alter the activity of histone-modifying enzymes by changing the conformational ensemble of the H3 tail, likely by directly associating with the nucleosomal DNA to increase tail accessibility.

Exogenous polyamines facilitate reprogramming.

Our data thus far show that polyamine depletion induces a lineage primed cell state by altering the activity of diverse histone-modifying enzymes. We wondered if exogenous polyamines might increase chromatin dynamics and facilitate reprogramming of terminally differentiated cells. Although cells pre-treated with DFMO for three days did not re-initiate proliferation after removal of drug, they did proliferate if media was supplemented with excess putrescine (Fig. 2F). ODC1 is a direct transcriptional target of c-Myc, one of the four Yamanaka reprogramming factors (*37*). We hypothesized that the role of c-Myc during reprogramming might be in part to increase polyamine biosynthesis, thereby facilitating the chromatin remodeling necessary for de-differentiation. To test this, we reprogrammed mouse embryonic fibroblasts expressing an Oct4-GFP reporter by doxycycline-inducible expression of either three (Oct4, Sox2, and Klf4; OSK) or four (Oct4, Sox2, Klf4, and Myc; OSKM) Yamanaka reprogramming factors in the presence of DFMO or putrescine. We assayed stable reprogramming efficiency by withdrawing cells from doxycycline for four days, then quantifying Oct4-GFP expression and colony number (Fig. 5A and B). Reprogramming with OSK resulted in low reprogramming efficiency and a small population of Oct4-expressing cells, while OSKM expression led to efficient reprogramming. Treatment of MYC-less OSK-expressing cells with putrescine increased Oct4-GFP reporter expression and reprogramming efficiency nearly to the levels of OSKM-reprogrammed fibroblasts (Fig. 5B-D). These data show that a primary role of c-Myc during reprogramming is its ability to increase polyamine biosynthesis.

Discussion

Our findings suggest that cells modulate their ability to rearrange chromatin structure by changing polyamine levels. Mechanistically, these data are consistent with a model whereby interactions between histone tails and the two gyres of DNA surrounding the nucleosome core limit the activity of chromatin-modifying enzymes. Polyamines, by neutralizing negative charges on the DNA backbone, can weaken this interaction, allowing increased tail accessibility that enables chromatin-modifying enzyme activity (Fig. 5E). This model is further supported by a) the lack of effects of polyamines when chromatin-modifying enzymes act on histone protein alone (Fig. 4G); b) that a histone modification that is not on the tail, but on the nucleosome core (H3K79 di-methylation), is unaffected by polyamine levels both *in vivo* and *in vitro* (Fig. S5K

and Fig. 4H); c) that incubation of nucleosomes with polyamines does not denature nucleosome structure (Fig. S5L); and d) that the addition of spermidine results in chemical shift perturbations consistent with increased H3 tail accessibility (Fig. 4I-J). Our work also underscores the importance of considering these abundant charged metabolites when modeling the structures of protein-protein and protein-nucleic acid interactions.

Some polyamine species are more efficient at increasing the enzymatic activity of certain chromatin-modifiers (e.g. putrescine for KDM4A and SIRT6 versus spermidine for GCN5 and G9a) (Fig. 4C-F). This may be attributable to the different charges present on putrescine (+2), spermidine (+3) and spermine (+4), and the differing electrostatic interactions between acetylated histone tails versus unmodified or methylated tails with DNA. Alternatively, steric hinderance might prevent some polyamine species from binding to different sites on the DNA gyres. Further structural studies and computational modeling will help explain this observation.

One emphasized role of polyamines is that spermidine acts as a substrate for the post-translational modification of eIF5A on lysine 50 (*14*, *38*). This modification, hypusination, enables translation elongation and termination of mRNAs encoding poly-proline tracts and other tri-peptide motifs (*23*, *24*, *39*). Previous studies have suggested that polyamine levels impact differentiation through their regulation of hypusination (*40*). The *in vivo* and *in vitro* effects of polyamines on chromatin structure do not prove that chromatin is the target of polyamines *vis a vis* differentiation. However, that inhibition of hypusination leads to impaired differentiation of the lines studied in this work, while DFMO and ODC1 loss favor a differentiation-like phenotype, argue that inhibition of hypusination is not mediating the cell state changes seen when polyamines are depleted.

Using clickable polyamine probes, we show that polyamines can concentrate in the nucleus. This finding is also supportive of their function as modulators of chromatin dynamics. Moreover, their enrichment in nucleoli suggests that they may be involved in ribosome biogenesis. This could either be through effects on chromatin dynamics, RNA polymerase I function or stabilization of RNA molecules. In support of the role of polyamines in ribosomal biogenesis, top gene sets upregulated in low polyamine conditions highlight ribosome biogenesis-related processes (Fig. S2H). Despite these effects on ribosome biology, ribosomes are long lived(*41*, *42*), and in the time required for polyamine depletion-driven differentiation-like changes, we do not see any change in ribosomal RNA concentration (Fig. S3F) or overall translation rate (Fig. S3B, C). Thus, the effects of polyamines on ribosome biogenesis are unlikely to explain the differen-

tiation-like state seen upon polyamine depletion.

We show that putrescine can substitute for MYC in the setting of reprogramming to pluripotency. Our model suggests that polyamines increase the efficiency of the chromatin remodeling reactions necessary for de-differentiation. Whether this increased efficiency is genome-wide, mediated through transcription factor-dependent recruitment of chromatin-modifying enzymes or through sub-nuclear compartment-driven localization of these metabolites is the topic of ongoing studies. Transformed cancer cells also take on a less differentiated state and in many cases upregulate polyamine biosynthesis. Accordingly, we found that depletion of polyamines led to decreased proliferation and induction of differentiation markers across a panel of cancer cell lines. One intriguing hypothesis is that by upregulating polyamine biosynthesis, transformed cells might acquire the capacity to alter chromatin structure, increasing lineage plasticity and allowing them to better adapt to diverse stressors and environments.

Methods and Materials

Cell culture and drug treatments

10T1/2 and C2C12 cells were cultured in DMEM with 10% FBS and 1% pen-strep. CRISPR knockout lines were generated by cloning pLentiCRISPRv2 (Addgene 98290) plasmids with sgRNA sequences targeting ODC1 or the Rosa safe harbor locus. 293T cells were transfected with PEI with the targeting plasmid and pMD2 (Addgene 12259) and psPAX2 (Addgene 12260) vectors to generate viral supernatants, which was harvested 24-48 hours after transfection and applied to target cells derived from single cell clones in the presence of 8 μg/mL polybrene. Knockout lines were generated from single cells clones after puromycin selection and passaged in media supplemented with 0.5 mM putrescine to rescue growth, then moved to media without putrescine for the duration of experiments. SK-N-BE(2) cells were cultured in DMEM F-12 media with 10% FBS and 1% pen-strep, COLO858 cells were cultured in RPMI with 5% FBS, 1% pen-strep and 1% sodium pyruvate, and Ki586 cells were cultured in RPMI with 20% FBS and 1% pen-strep. Cells were treated with 1 mM DFMO, 1 mM putrescine, 0.5 μM GC7, 1 μM UNC0368, 0.5 mM octyl-R-2HG, 25 μM JG2016, 0.5 μM Vorinostat, or 1 μM EPZ5676. For differentiation experiments, confluent 10T cells were exposed to chondrocyte differentiation media (DMEM containing 1% FBS, 1% pen-strep, 3e-8M sodium selenite, 10 μg/mL insulin, 1e-8M dexamethasone, 10 μg/mL transferrin, and 100ng/mL BMP-2). Confluent C2C12 cells were exposed to myotube differentiation media (DMEM containing 1% pen-strep and 2% horse serum). Differentiation media was refreshed every two to three days. For growth curves, 15,000 cells were plated in triplicate, and counted using a Beckman-Coulter Multisizer 3. For viability analysis, cells were stained with Trypan Blue, and counted using a Countess 3 Automated Cell Counter (ThermoFisher). All lines were determined to be mycoplasma free using MycoAlert Detection Kit (Lonza).

Western Blots

Protein lysates were harvested from cells on ice with 1X RIPA buffer supplemented with protease and phosphatase inhibitors (Thermo Fisher # 1860932 and Thermo Fisher # 78428, respectively). For experiments in which histone marks were assayed, lysates were harvested in 1X RIPA buffer with 10% SDS and sonicated with a Bioruptor Plus (Diagenode). Protein was separated on NuPAGE 4-12% Bis-Tris gels (Invitrogen NP0336), blocked in 5% non-fat milk, and incubated with primary antibodies. After washing and secondary antibody incubation, blots were incubated in 1-shot ECL solution (Kindle Biosciences LLC) and imaged with a ChemiDoc MP Imaging System (BioRad).

EdU and OPP incorporation and flow cytometry

Cells were treated for 25 minutes with 20 μM EdU or 20 μM OPP (Thermo Fisher C10456). Following this pulse, EdU-labeled cells were harvested, washed three times with 1% BSA in PBS, and fixed with 4% paraformaldehyde (PFA). After fixation, cells were permeabilized with 0.5% Triton X-100 in PBS, washed three times, and incubated in click chemistry reaction mix (2 mM CuSO4, 8 μM sulfo-azide dye, 20 mg/mL ascorbic acid in PBS) for 30 minutes in the dark. Cells were then washed, incubated in Hoechst (4 μg/mL), and EdU incorporation was assayed by flow cytometry (NovoCyte Quanteon).

OPP-pulsed cells were fixed in ice-cold methanol for 10 minutes at –20°C, washed in 1% BSA in PBS, and permeabilized with 0.5% Triton X-100. Cells were stained with homemade click chemistry reaction mix for thirty minutes, washed, and analyzed by flow cytometry (NovoCyte Quanteon).

Gas chromatography mass spectrometry

GC-MS data collected over a time course of zebrafish embryonic development was analyzed from Dhillon et al., 2019(*43*).

For extraction, chromatography and mass spectrometry analysis, cells were harvested in 80% Methanol, Optima LC/MS Grade, (Fisher Chemical) overnight at -80˚C and dried using a Speed Vac Vacuum Concentrator (Savant) attached to a Universal Vacuum System (Savant). Samples were resuspended in an extraction buffer (10% NaCl solution made pH 1 with 0.5 M HCl) and polyamines were extracted with diethyl ether. Polyamines were derivatized by extracting two times with 15% ethyl chloroformate in diethyl ether and dried under a nitrogen stream. After another round of derivatization with trifluoroacetic anhydride in ethyl acetate, samples were dried under a nitrogen stream and resuspended in ethyl acetate. Polyamines were measured with the Agilent 8890/5977C gas chromatography/mass selective detector (GC/MSD).

RNAseq, ATACseq, and MNase digestion

RNAseq data was analyzed from the following repositories: GSE129957, GSE99399, GSE106292, GSE122380, and the LIBD Stem Cell Browser (*44*).

RNA was harvested from cells (RNeasy Mini Kit, Qiagen 74104), and quality control was performed by Tapestation analysis (Agilent). Libraries were prepared with the TruSeq Stranded mRNA Library Prep Kit (Illumina) and sequenced on an AVITI system (Element Biosciences) using paired-end sequencing. bases-2fastq was used to demultiplex the data, and reads were mapped to the mouse genome (GRCm10) using

kallisto. Count matrices were analyzed in R using DESeq2.

ATACseq library preparation was carried out as previously described (*45*) and included a spike-in of 0.1 ng E. coli DNA per sample (EpiCypher # 18-1401). Libraries were amplified with NEBNext Multiplex Oligos (Illumina), and quality control was performed with Tapestation (Agilent) and KAPA library quantification (Roche). Libraries were sequenced on an AVITI system (Element Biosciences) using paired-end sequencing, and quality control was performed using FASTQC. Reads were trimmed using Trimgalore, and aligned to GRCm10 and the NCBI E. coli K12 genome using Bowtie2. Sorting and duplicate removal was performed using Samtools and Picard, and peaks were called with MACS2. Depth normalization to E. coli internal standards, and differential peak analysis, was performed using DiffBind. Peaks were annotated with ChipSeeker and CHIPpeakAnno, and reads were indexed for visualization with Samtools.

For MNase digestion experiments, nuclei from 147,000 cells per sample were incubated in 1 U MNase (ThermoFisher, EN0181) per million cells for 15 minutes at 37°C. DNA was extracted and quantified on a Qubit (ThermoFisher). 3ng DNA per sample was analyzed with a high sensitivity Tapestation (Agilent).

Polyamine probe and microscopy

Putrescine, spermidine, and spermine azide probes were synthesized as previously described(*46*), without the addition of the BoDiPY moiety. Probes were resuspended in media at 10 μM and applied to live cells for two hours. Cells were then washed, fixed with 4% paraformaldehyde, permeabilized with 0.1% Triton-X in PBS, and incubated in homemade click chemistry reaction cocktail (2 mM $CuSO_4$, 8 μM alkyne-conjugated fluorophore, 20 mg/mL ascorbic acid) for 30 minutes. Following click chemistry reactions, cells were stained with Hoechst or DAPI, and imaged on a Zeiss LSM 780 confocal microscope.

For zebrafish probe experiments, AB wildtype embryos were manually dechorionated at the four-cell stage and moved into water containing 10 μM polyamine probe for 2 hours. Embryos were then fixed for 20 minutes with 4% PFA, permeabilized with 0.1% Triton X-100 in PBS, incubated in homemade click chemistry reaction cocktail with an alkyne-conjugated fluorophore for 30 minutes, and then DNA was stained with Hoechst. Yolk was removed by manual dissection and embryos were mounted for imaging on a Zeiss LSM 780 confocal microscope. The Institutional Animal Care and Use Committees of Columbia University approved all zebrafish experiments.

In vitro enzymatic assays

All *in vitro* reactions were carried out with 1 µg nucleosome or histone protein substrate and 2.8 µg enzyme in 40 µL reaction buffer at 37°C for one hour. Reactions were halted by addition of NuPAGE sample buffer, boiled at 95°C for 5 minutes, and then split in two and run on separate NuPAGE 4-12% Bis-Tris gels for analysis by western blot. *In vitro* demethylase reaction buffer contained 50 mM Tris-HCl pH 8.0, 5% glycerol, 2 mM ascorbate, 1 mM alpha-ketoglutarate, 100 µM $FeSO_4$, and protease inhibitor. *In vitro* methyltransferase reaction buffer contained 50 mM Tris-HCl pH 8.0, 5 mM $MgCl_2$, 10 µM SAM, 4 mM DTT, and protease inhibitor. *In vitro* deacetylase reaction buffer contained 25 mM Tris-HCl pH 8.0, 50 mM NaCl, 1 mM DTT, 5 mM NAD+ and protease inhibitor. *In vitro* acetylase reaction buffer contained 50 mM Tris-HCl pH 8.0, 5% glycerol, 1 mM DTT, 50 mM NaCl, 100 µM acetyl CoA, and protease inhibitor.

To assess nucleosome integrity after polyamine incubation, mononucleosomes were incubated for one hour at 37°C in the presence of 100 µM putrescine, spermidine, or spermine. A digested control sample was processed with the Zymo Research Clean and Concentrate Kit. Samples were run on a 1.5% agarose gel, DNA was stained with ethidium bromide, and the gel was imaged on a ChemiDoc MP Imaging System (BioRad).

Histone purification and nucleosome reconstitution for NMR

Histones and DNA were purified and reconstituted as outlined in Dyer et al (*47*). Unmodified human histones (H2A.1 Uniprot accession P0C0S8, H2B.1C Uniprot accession P62807, H4 Uniprot accession P62805, and H3.2 Uniprot accession Q71DI3 with C110A and G102A) were expressed in Rosetta 2 (DE3) pLysS (Novagen) or BL21 (DE3) (New England Biolabs) chemically competent E. coli. Unlabeled growths were carried out in LB and induced at OD600~0.4 with 0.2mM (for H4) or 0.4mM (for H2A, H2B, and H3) IPTG for 3-4 hours. ^{15}N-isotopically enriched H3 was grown in M9 minimal media supplemented with vitamin (Centrum) and 1g L-$^{15}NH_4Cl$. Histones were extracted from inclusion bodies and purified via ion exchange chromatography. Histones were validated using ESI mass spectrometry (Fig. S6C). For DNA purification, a plasmid containing 37 repeats of the 147 bp Widom 601 sequence (ATCGAGAATC CCGGTGCCGA GGCCGCTCAA TTGGTCGTAG ACAGCTCTAG CACCGCTTAA ACGCACGTAC GCGCTGTCCC CCGCGTTTTA ACCGCCAAGG GGATTACTCC CTAGTCTCCA GGCACGTGTC AGATATATAC ATCCGAT) was amplified in E. coli and purified via alkaline lysis methods. The 601 repeats were released by cleavage with EcoRV and purified from parent plasmid by polyethylene glycol precipitation. Nucleosome reconstitutions were prepared by refolding tetramer (with equimolar ratios of H3 and H4) and dimer (with equimolar ratios of H2A and H2B) separately. Tetramer, dimer, and 601 DNA were then mixed together at a 1:2.2:1 molar ratio. Both mixtures were then desalted using a linear gradient from 2 M to 150 mM NaCl over 36-48

hours, followed by dialysis against 0.5xTE. Samples were then purified with a 10-40% sucrose gradient, which separates residual free 601 DNA and any subnucleosomal particles (i.e. tetrasome and hexasome). Native- and SDS-PAGE were used to assess the formation of nucleosomes along with histone composition (see Fig. S6A). Bands were visualized with ethidium bromide or Coomassie for native and denaturing gels, respectively. Nucleosomes were then dialyzed into 20 mM MOPS pH 7, 100 mM NaCl, 1 mM DTT, 1 mM EDTA for the purposes of NMR titrations. Concentrations were determined via UV-vis spectroscopy using the absorbance from the 601 DNA (calculated ε260 = 2,312,300.9 $M^{-1}cm^{-1}$). Samples were diluted into 2M NaCl prior to concentration measurements in order to promote nucleosome disassembly for more accurate concentration determination.

NMR Titration

^{1}H,^{15}N heteronuclear single quantum coherence ($^{1}H^{15}N$-HSQC) spectra of ^{15}N-labelled ^{15}N-H3-NCP (128 μM) in 20 mM MOPS pH 7, 100 mM NaCl, 1 mM DTT, 1 mM EDTA, and 10% D_2O were measured at varying spermidine trichloride concentrations. All the HSQC spectra were measured at 37°C on a Bruker Avance Neo 600 MHz spectrometer equipped with a room temperature probe. The NMR spectra were processed in NMRPipe and analyzed using Sparky (*48*). The normalized chemical shift difference (Δδ) was calculated using the following equation:

$$\Delta\delta = \sqrt{(\Delta\delta_H)^2 + (0.154\Delta\delta_N)^2}$$

Where $\Delta\delta_H$ and $\Delta\delta_N$ are the observed changes in the ^{1}H and ^{15}N chemical shifts, respectively, upon addition of spermidine trichloride.

Reprogramming

Mouse embryonic fibroblasts (MEFs) expressing either doxycycline-inducible OSK or OSKM were reprogrammed as previously described (*49*). Briefly, cells were seeded on a layer of feeder MEFs, then transferred into induction media (DMEM with 15% FBS, 1% non-essential amino acids, 1% GlutaMAX, beta-marcaptoethanol and 1000 U/mL LIF) containing 1 mg/mL doxycycline and either 1 mM DFMO or 1 mM putrescine. Media was refreshed every two days for twelve days, and then cells were moved into induction media without doxycycline for four days. Doxycycline-independent GFP-positive colonies were counted manually, and then live cells were dissociated for analysis by flow cytometry on a NovoCyte Quanteon.

Acknowledgements

We thank C. Chio (Columbia University) and C. Lu (Columbia University) for antibody reagents and E. Mikhail Yohannan Cheria (Columbia University) for assistance with GCMS. Three and four factor reprogrammable fibroblasts were a gift from M. Stadtfeld (Weill Cornell Medical College). Flow cytometry and confocal microscopy were performed in the Columbia Stem Cell Initiative Flow Cytometry Institutional Core facility and the Columbia Medicine Microscopy Core. The histone acetyl-transferase inhibitor JG2016 was a gift from J. Gruber (UT Southwestern Medical Center). We thank C. Chio, C. Lu, S. Sternberg and L. Johnston for critical reading of the manuscript.

Funding

J.M.S. was supported by W81XWH-21-1-0292 US Army Medical Research and Development Command (USAMRDC), Department of Defense. M.E.B. was supported by a Hope Funds for Cancer Research Postdoctoral Fellowship. Work in the Smeeton lab was supported by the National Institute of Dental & Craniofacial Research (NIH; DP2DE032725). Work in the Musselman laboratory is funded by the National Institutes of Health (NIH; R35GM128705). Operation of the NMR spectrometers is funded by the National Institutes of Health (NIH; P30 CA046934 and S10 OD014010-01).

Author Contributions

Conceptualization: MEB, JMS

Methodology: MEB, GF, AJS, SO, AG, RS, JC, SV, MHK, JS, SA, HAF, CM

Investigation: MEB, GF, AJS, SO, AG, RS, JC, MHK, SA, HAF

Data Curation: MEB, GF, AJS, SV, MHK, JS, SA, CM, JMS

Formal Analysis: MEB, GF, AJS, SV, JS, CM, JMS

Visualization: MEB, CM, JMS

Funding Acquisition: MEB, JS, CM, JMS

Project Administration: JMS

Supervision: JMS

Writing – original draft: MEB, JMS

Writing – review & editing: MEB, JMS

Competing Interests

MEB and JMS are authors of a patent submitted by Columbia University related to this work. All other

authors declare that they have no competing interests.

Data and Materials Availability

All data and materials are available upon request. Sequencing data are deposited with the NCBI GEO (accession pending).

References

1. C. E. Holbert, M. T. Cullen, R. A. Casero, T. M. Stewart, Polyamines in cancer: integrating organismal metabolism and antitumour immunity. *Nat Rev Cancer* **22**, 467–480 (2022).

2. L. Alhonen-Hongisto, P. Seppänen, J. Jänne, Intracellular putrescine and spermidine deprivation induces increased uptake of the natural polyamines and methylglyoxal bis(guanylhydrazone). *Biochem. J.* **192**, 941–945 (1980).

3. W. W. Chen, E. Freinkman, T. Wang, K. Birsoy, D. M. Sabatini, Absolute Quantification of Matrix Metabolites Reveals the Dynamics of Mitochondrial Metabolism. *Cell* **166**, 1324 1337.e11 (2016).

4. R. M. Ray, B. J. Zimmerman, S. A. McCormack, T. B. Patel, L. R. Johnson, Polyamine depletion arrests cell cycle and induces inhibitors p21Waf1/Cip1, p27Kip1, and p53 in IEC-6 cells. *Am. J. Physiol.-Cell Physiol.* **276**, C684–C691 (1999).

5. B. F. Cheetham, An Inhibitor of Polyamine Synthesis Arrests Cells at an Earlier Stage of G1 than Does Calcium Deprivation. *Mol. Cell. Biol.* **3**, 480–483 (1983).

6. O. Heby, G. Andersson, J. W. Gray, Interference with S and G2 phase progression by polyamine synthesis inhibitors. *Exp. Cell Res.* **111**, 461–464 (1978).

7. A. M. Jetten, J. E. Shirley, Inhibition of ornithine decarboxylase by retinoic acid and difluoromethylornithine in relation to their effects on differentiation and proliferation. *Exp Cell Res* **156**, 221–230 (1985).

8. S. M. Oredsson, M. Billgren, O. Heby, Induction of F9 embryonal carcinoma cell differentiation by inhibition of polyamine synthesis. *Eur J Cell Biol* **38**, 335–43 (1985).

9. S. K. Choudhary, D. Sharma, A. Dixit, D,L-alpha-difluoromethylornithine, an irreversible inhibitor of ornithine decarboxylase, induces differentiation in MEL cells. *Cell Biol. Int.* **23**, 489–495 (1999).

10. C. Bello-Fernandez, G. Packham, J. L. Cleveland, The ornithine decarboxylase gene is a transcriptional target of c-Myc. *Proc National Acad Sci* **90**, 7804–7808 (1993).

11. J. A. Nilsson, U. B. Keller, T. A. Baudino, C. Yang, S. Norton, J. A. Old, L. M. Nilsson, G. Neale, D. L. Kramer, C. W. Porter, J. L. Cleveland, Targeting ornithine decarboxylase in Myc-induced lymphomagenesis prevents tumor formation. *Cancer Cell* **7**, 433–444 (2005).

12. M. D. Hogarty, M. D. Norris, K. Davis, X. Liu, N. F. Evageliou, C. S. Hayes, B. Pawel, R. Guo, H. Zhao, E. Sekyere, J. Keating, W. Thomas, N. C. Cheng, J. Murray, J. Smith, R. Sutton, N. Venn, W. B. London, A. Buxton, S. K. Gilmour, G. M. Marshall, M. Haber, ODC1 Is a Critical Determinant of MYCN Oncogenesis and a Therapeutic Target in Neuroblastoma. *Cancer Res* **68**, 9735–9745 (2008).

13. M. H. Park, H. L. Cooper, J. E. Folk, Identification of hypusine, an unusual amino acid, in a protein from

human lymphocytes and of spermidine as its biosynthetic precursor. *Proc. Natl. Acad. Sci.* **78**, 2869–2873 (1981).

14. H. L. Cooper, M. H. Park, J. E. Folk, B. Safer, R. Braverman, Identification of the hypusine-containing protein hy+ as translation initiation factor eIF-4D. *Proc National Acad Sci* **80**, 1854–1857 (1983).

15. A. N. Lopatin, E. N. Makhina, C. G. Nichols, Potassium channel block by cytoplasmic polyamines as the mechanism of intrinsic rectification. *Nature* **372**, 366–369 (1994).

16. B. G. Feuerstein, N. Pattabiraman, L. J. Marton, Molecular mechanics of the interactions of spermine with DNA: DNA bending as a result of ligand binding. *Nucleic Acids Res* **18**, 1271–1282 (1990).

17. A. Kanemura, Y. Yoshikawa, W. Fukuda, K. Tsumoto, T. Kenmotsu, K. Yoshikawa, Opposite effect of polyamines on In vitro gene expression: Enhancement at low concentrations but inhibition at high concentrations. *Plos One* **13**, e0193595 (2018).

18. K. Kleppe, A. Osland, V. Fosse, R. Male, I. Lossius, D. Helland, J. R. Lillehaug, A. J. Raae, R. K. Kleppe, I. F. Nes, Effect of polyamines on enzymes involved in DNA repair. *Med Biol* **59**, 374–80 (1981).

19. R. D. Snyder, Polyamine depletion is associated with altered chromatin structure in HeLa cells. *Biochem J* **260**, 697–704 (1989).

20. G. G. Chen, G. Turecki, O. A. Mamer, A quantitative GC-MS method for three major polyamines in postmortem brain cortex. *J. Mass Spectrom.* **44**, 1203–1210 (2009).

21. S.-H. Choi, S.-W. Kim, D.-H. Choi, B.-H. Min, B.-G. Chun, Polyamine-depletion induces p27Kip1 and enhances dexamethasone-induced G1 arrest and apoptosis in human T lymphoblastic leukemia cells. *Leuk. Res.* **24**, 119–127 (2000).

22. V. Pelechano, P. Alepuz, eIF5A facilitates translation termination globally and promotes the elongation of many non polyproline-specific tripeptide sequences. *Nucleic Acids Res.* **45**, 7326–7338 (2017).

23. A. P. Schuller, C. C.-C. Wu, T. E. Dever, A. R. Buskirk, R. Green, eIF5A Functions Globally in Translation Elongation and Termination. *Mol. Cell* **66**, 194-205.e5 (2017).

24. E. Gutierrez, B.-S. Shin, C. J. Woolstenhulme, J.-R. Kim, P. Saini, A. R. Buskirk, T. E. Dever, eIF5A Promotes Translation of Polyproline Motifs. *Mol. Cell* **51**, 35–45 (2013).

25. M. H. Park, E. C. Wolff, Hypusine, a polyamine-derived amino acid critical for eukaryotic translation. *J. Biol. Chem.* **293**, 18710–18718 (2018).

26. K. Pakos-Zebrucka, I. Koryga, K. Mnich, M. Ljujic, A. Samali, A. M. Gorman, The integrated stress response. *EMBO Rep.* **17**, 1374–1395 (2016).

27. J. Yoo, H. Kim, A. Aksimentiev, T. Ha, Direct evidence for sequence-dependent attraction between double-stranded DNA controlled by methylation. *Nat. Commun.* **7**, 11045 (2016).

28. W. Pan, J. Zhou, Y. Yin, H. Wen, D. Liang, Local de-condensation of double-stranded DNA in opposite-

ly charged polyelectrolyte as induced by spermidine. *Soft Matter* **11**, 4705–4709 (2015).

29. K. R. Karch, M. Coradin, L. Zandarashvili, Z.-Y. Kan, M. Gerace, S. W. Englander, B. E. Black, B. A. Garcia, Hydrogen-Deuterium Exchange Coupled to Top- and Middle-Down Mass Spectrometry Reveals Histone Tail Dynamics before and after Nucleosome Assembly. *Structure* **26**, 1651-1663.e3 (2018).

30. S. R. Daigle, E. J. Olhava, C. A. Therkelsen, C. R. Majer, C. J. Sneeringer, J. Song, L. D. Johnston, M. P. Scott, J. J. Smith, Y. Xiao, L. Jin, K. W. Kuntz, R. Chesworth, M. P. Moyer, K. M. Bernt, J.-C. Tseng, A. L. Kung, S. A. Armstrong, R. A. Copeland, V. M. Richon, R. M. Pollock, Selective Killing of Mixed Lineage Leukemia Cells by a Potent Small-Molecule DOT1L Inhibitor. *Cancer Cell* **20**, 53–65 (2011).

31. L. Imre, E. F. Niaki, R. Bosire, P. Nanasi, P. Nagy, Z. Bacso, N. Hamidova, Y. Pommier, A. Jordan, G. Szabo, Nucleosome destabilization by polyamines. *Arch. Biochem. Biophys.* **722**, 109184 (2022).

32. A. Stützer, S. Liokatis, A. Kiesel, D. Schwarzer, R. Sprangers, J. Söding, P. Selenko, W. Fischle, Modulations of DNA Contacts by Linker Histones and Post-translational Modifications Determine the Mobility and Modifiability of Nucleosomal H3 Tails. *Mol. Cell* **61**, 247–259 (2016).

33. E. A. Morrison, S. Bowerman, K. L. Sylvers, J. Wereszczynski, C. A. Musselman, The conformation of the histone H3 tail inhibits association of the BPTF PHD finger with the nucleosome. *eLife* **7**, e31481 (2018).

34. H. Ohtomo, S. Ito, N. J. McKenzie, M. Uckelmann, M. Wakamori, H. Ehara, A. Furukawa, Y. Tsunaka, M. Shibata, S. Sekine, T. Umehara, C. Davidovich, H. Koseki, Y. Nishimura, H2A Ubiquitination Alters H3-tail Dynamics on Linker-DNA to Enhance H3K27 Methylation. *J. Mol. Biol.* **435**, 167936 (2023).

35. C. E. Jennings, C. J. Zoss, E. A. Morrison, Arginine anchor points govern H3 tail dynamics. *Front. Mol. Biosci.* **10**, 1150400 (2023).

36. E. A. Morrison, L. Baweja, M. G. Poirier, J. Wereszczynski, C. A. Musselman, Nucleosome composition regulates the histone H3 tail conformational ensemble and accessibility. *Nucleic Acids Res.* **49**, 4750–4767 (2021).

37. K. Takahashi, S. Yamanaka, Induction of pluripotent stem cells from mouse embryonic and adult fibroblast cultures by defined factors. *Cell* **126**, 663 676 (2006).

38. M. K. Chattopadhyay, M. H. Park, H. Tabor, Hypusine modification for growth is the major function of spermidine in Saccharomyces cerevisiae polyamine auxotrophs grown in limiting spermidine. *Proc. Natl. Acad. Sci.* **105**, 6554–6559 (2008).

39. V. Pelechano, P. Alepuz, eIF5A facilitates translation termination globally and promotes the elongation of many non polyproline-specific tripeptide sequences. *Nucleic Acids Res.* **45**, 7326–7338 (2017).

40. D. J. Puleston, F. Baixauli, D. E. Sanin, J. Edwards-Hicks, M. Villa, A. M. Kabat, M. M. Kamiński, M. Stanckzak, H. J. Weiss, K. M. Grzes, K. Piletic, C. S. Field, M. Corrado, F. Haessler, C. Wang, Y. Musa, L.

Schimmelpfennig, L. Flachsmann, G. Mittler, N. Yosef, V. K. Kuchroo, J. M. Buescher, S. Balabanov, E. J. Pearce, D. R. Green, E. L. Pearce, Polyamine metabolism is a central determinant of helper T cell lineage fidelity. *Cell*, doi: 10.1016/j.cell.2021.06.007 (2021).

41. A. R. Dörrbaum, L. Kochen, J. D. Langer, E. M. Schuman, Local and global influences on protein turnover in neurons and glia. *eLife* **7**, e34202 (2018).

42. M. K. Doherty, D. E. Hammond, M. J. Clague, S. J. Gaskell, R. J. Beynon, Turnover of the Human Proteome: Determination of Protein Intracellular Stability by Dynamic SILAC. *J. Proteome Res.* **8**, 104–112 (2009).

43. S. S. Dhillon, F. Torell, M. Donten, K. Lundstedt-Enkel, K. Bennett, S. Rännar, J. Trygg, T. Lundstedt, Metabolic profiling of zebrafish embryo development from blastula period to early larval stages. *PLoS ONE* **14**, e0213661 (2019).

44. E. E. Burke, J. G. Chenoweth, J. H. Shin, L. Collado-Torres, S.-K. Kim, N. Micali, Y. Wang, C. Colantuoni, R. E. Straub, D. J. Hoeppner, H.-Y. Chen, A. Sellers, K. Shibbani, G. R. Hamersky, M. D. Bustamante, B. N. Phan, W. S. Ulrich, C. Valencia, A. Jaishankar, A. J. Price, A. Rajpurohit, S. A. Semick, R. W. Bürli, J. C. Barrow, D. J. Hiler, S. C. Page, K. Martinowich, T. M. Hyde, J. E. Kleinman, K. F. Berman, J. A. Apud, A. J. Cross, N. J. Brandon, D. R. Weinberger, B. J. Maher, R. D. G. McKay, A. E. Jaffe, Dissecting transcriptomic signatures of neuronal differentiation and maturation using iPSCs. *Nat. Commun.* **11**, 462 (2020).

45. M. R. Corces, A. E. Trevino, E. G. Hamilton, P. G. Greenside, N. A. Sinnott-Armstrong, S. Vesuna, A. T. Satpathy, A. J. Rubin, K. S. Montine, B. Wu, A. Kathiria, S. W. Cho, M. R. Mumbach, A. C. Carter, M. Kasowski, L. A. Orloff, V. I. Risca, A. Kundaje, P. A. Khavari, T. J. Montine, W. J. Greenleaf, H. Y. Chang, An improved ATAC-seq protocol reduces background and enables interrogation of frozen tissues. *Nat Methods* **14**, 959 962 (2017).

46. R. Vanhoutte, J. P. Kahler, S. Martin, S. van Veen, S. H. L. Verhelst, Clickable Polyamine Derivatives as Chemical Probes for the Polyamine Transport System. *Chembiochem* **19**, 907–911 (2018).

47. P. N. Dyer, R. S. Edayathumangalam, C. L. White, Y. Bao, S. Chakravarthy, U. M. Muthurajan, K. Luger, Reconstitution of Nucleosome Core Particles from Recombinant Histones and DNA. *Methods Enzym.* **375**, 23–44 (2003).

48. F. Delaglio, S. Grzesiek, G. W. Vuister, G. Zhu, J. Pfeifer, A. Bax, NMRPipe: A multidimensional spectral processing system based on UNIX pipes. *J. Biomol. NMR* **6**, 277–293 (1995).

49. S. E. Vidal, B. Amlani, T. Chen, A. Tsirigos, M. Stadtfeld, Combinatorial Modulation of Signaling Pathways Reveals Cell-Type-Specific Requirements for Highly Efficient and Synchronous iPSC Reprogramming. *Stem Cell Rep.* **3**, 574–584 (2014).

Figure Legends

Figure 1

A) Polyamines are synthesized by the irreversible decarboxylation of ornithine by ornithine decarboxylase (ODC1), which is a direct transcriptional target of MYC, and inhibited by the drug difluoromethylornithine (DFMO).

B) ODC1 expression from publicly-available RNAseq data collected over time courses of adipocyte, osteoblast, chondrocyte, neuronal, myotube, and hematopoietic differentiation.

C) Western blots showing induction of the chondrocyte marker Aggrecan in 10T1/2 cells following seven days of treatment with chondrocyte differentiation media, and induction of the myotube markers Myosin Heavy Chain and MyoG in C2C12 cells after seven days of treatment with myotube differentiation media.

D) Quantification of relative polyamine levels over a time course of differentiation in 10T1/2 and C2C12 cells. Abundance of each polyamine species was normalized to cell number. Error bars correspond to standard error. P values calculated by Dunn's test.

Figure 2

A) Control (sgRosa) and ODC1 knockout (sgODC1) cells were plated in media containing vehicle, 1 mM DFMO, or 1 mM putrescine, and cells were counted one, three, and four days after seeding. Data presented are mean +/- standard error of three biological replicates. P values calculated by Dunn's test.

B) Relative putrescine concentrations in control (sgRosa) and ODC1 knockout (sgODC1) cells following three days of growth in putrescine-free media. Putrescine abundance was normalized to cell counts. Error bars correspond to standard error. P values calculated by one-tailed t-test.

C) Morphology of control (sgRosa) and ODC1 knockout (sgODC1) cells following three days of indicated treatments (1 mM DFMO, 1 mM putrescine). Scale bar is 275 μM.

D) Principal component analysis of RNAseq data from control (sgRosa) and ODC1 knockout (sgODC1) cells. RNA was extracted from cells following three days of indicated treatments (1 mM DFMO, 1 mM putrescine).

E) Gene set enrichment analysis comparing low-polyamine samples (control cells treated with DFMO, and ODC1 knockout cells treated with vehicle or DFMO) to high-polyamine samples (control cells treated with vehicle or putrescine, and ODC1 knockout cells treated with putrescine).

F) 10T1/2 cells were treated with either vehicle or DFMO-containing media and moved into indicat-

ed treatments after three days. Cells were counted six days after plating (three days after media change). Data presented are mean +/- standard error of three biological replicates. P values calculated by Dunn's test.

G) Western blots showing markers of differentiation in progenitor and transformed cell lines. 10T1/2 cells were treated with the indicated treatments (1 mM DFMO) in growth media for 24 hours and then moved to differentiation media for 24 hours. C2C12 cells were treated with the indicated treatments (1 mM DFMO, 1 mM putrescine) in differentiation media. All transformed cell lines were treated with 1 mM DFMO in growth media.

Figure 3

A) Structure of the putrescine-azide probe.

B) Intracellular localization of the putrescine probe in 10T1/2 cells was visualized by confocal microscopy following three days of the indicated treatments (1 mM DFMO, 1 mM putrescine). Scale bars are 5 μM.

C) Co-localization of putrescine probe fluorescence and anti-NPM1 immunofluorescence staining visualized by confocal microscopy in control (sgRosa) or ODC1 knockout (sgODC1) cells following three days of treatment with putrescine-free media. Scale bars are 5 μM.

D) Line scan quantification of fluorescence intensity across region indicated in panel C.

E) Putrescine localization in control (sgRosa) 10T1/2 cells treated with RNAse (where indicated) for thirty minutes prior to conjugation to fluorophore alkyne. Scale bars are 5 μM.

F) Co-localization of spermidine (top) and spermine (bottom) probe fluorescence and anti-NPM1 immunofluorescence staining in control 10T1/2 cells visualized by confocal microscopy. Scale bars are 5 μM.

Figure 4

A) Distribution of the fold change in peak accessibility in control 10T1/2 cells treated with either 1 mM DFMO or 1 mM putrescine for three days as determined by ATACseq.

B) Western blots showing abundance of H3K27ac following treatment with a histone acetyltransferase inhibitor (25 μM JG2016) or histone deacetylase inhibitor (0.5 μM Vorinostat) in the presence or absence of 1 mM DFMO. Cells were pre-treated with DFMO for 24 hours, and then transferred into media with HAT and HDAC inhibitors with or without DFMO for 24 hours.

C) Western blot showing H3K9me2 abundance following *in vitro* demethylase reactions. Recombinant KDM4A was incubated in the presence of H3K9me2-decorated nucleosomes and increasing

concentrations of putrescine for one hour at 37°C. Reactions were quenched with SDS, boiled, and assessed by western blot.

D) Western blot showing H3K18ac abundance following *in vitro* deacetylase reactions. Recombinant Sirt6 was incubated in the presence of H3K18ac-decorated nucleosomes and 100 μM putrescine, spermidine, or spermine for one hour at 37°C. Reactions were quenched with SDS, boiled, and assessed by western blot.

E) Western blot showing H3K18ac abundance following *in vitro* acetyltransferase reactions. Recombinant GCN5 was incubated in the presence of bulk mononucleosomes extracted from HeLa cells and 100 μM putrescine, spermidine, or spermine for one hour at 37°C. Reactions were quenched with SDS, boiled, and assessed by western blot.

F) Western blot showing H3K9me2 abundance following *in vitro* methyltransferase reactions. Recombinant G9a was incubated in the presence of recombinant mononucleosomes and 100 μM putrescine, spermidine, or spermine for one hour at 37°C. Reactions were quenched with SDS, boiled, and assessed by western blot.

G) Western blot showing H318ac abundance following *in vitro* acetyltransferase reactions. Recombinant GCN5 was incubated in the presence of purified H3 protein without DNA and 100 μM putrescine, spermidine, or spermine for one hour at 37°C. Reactions were quenched with SDS, boiled, and assessed by western blot.

H) Western blot showing H3K79me2 abundance following *in vitro* methyltransferase reactions. Recombinant DOT1L was incubated in the presence of unmodified mononucleosomes and 100 μM putrescine, spermidine, or spermine for one hour at 37°C. Reactions were quenched with SDS, boiled, and assessed by western blot.

I) Overlay of the selected regions in the ^{1}H,^{15}N-HSQC spectra of ^{15}N-H3-NCP (128 μM) with (dark blue) and without (light blue) 512 μM spermidine trichloride.

J) Normalized chemical shift difference as a function of H3 tail residues in ^{15}N-H3-NCP at 512 μM spermidine trichloride concentration. The dotted line represents the average shift.

Figure 5

A) Mouse embryonic fibroblasts expressing GFP under the control of the endogenous Oct4 locus were reprogrammed with either three (Oct4, Sox2, Klf4; OSK), or four (Oct4, Sox2, Klf4, Myc; OSKM) Yamanaka factors.

B) Top: timeline of reprogramming experiments: MEFs were plated on a feeder layer and treated with doxycycline to induce OSK and OSKM expression. Doxycycline was removed at day 12 and dox-

ycycline-independent colonies assessed after four days. Bottom: Oct4-GFP expression quantified by flow cytometry of indicated cells.

C) Morphology and Oct4-GFP expression of reprogrammed colonies following the indicated treatments. Scale bars are 275 μM.

D) Reprogramming efficiency quantified by calculating the number of Oct4-GFP-positive colonies following indicated treatments as a percentage of initial cells plated. Each data point represents one biological replicate. P values calculated by Dunn's test.

E) Model of electrostatic interactions between polyamines and nucleosomal DNA.

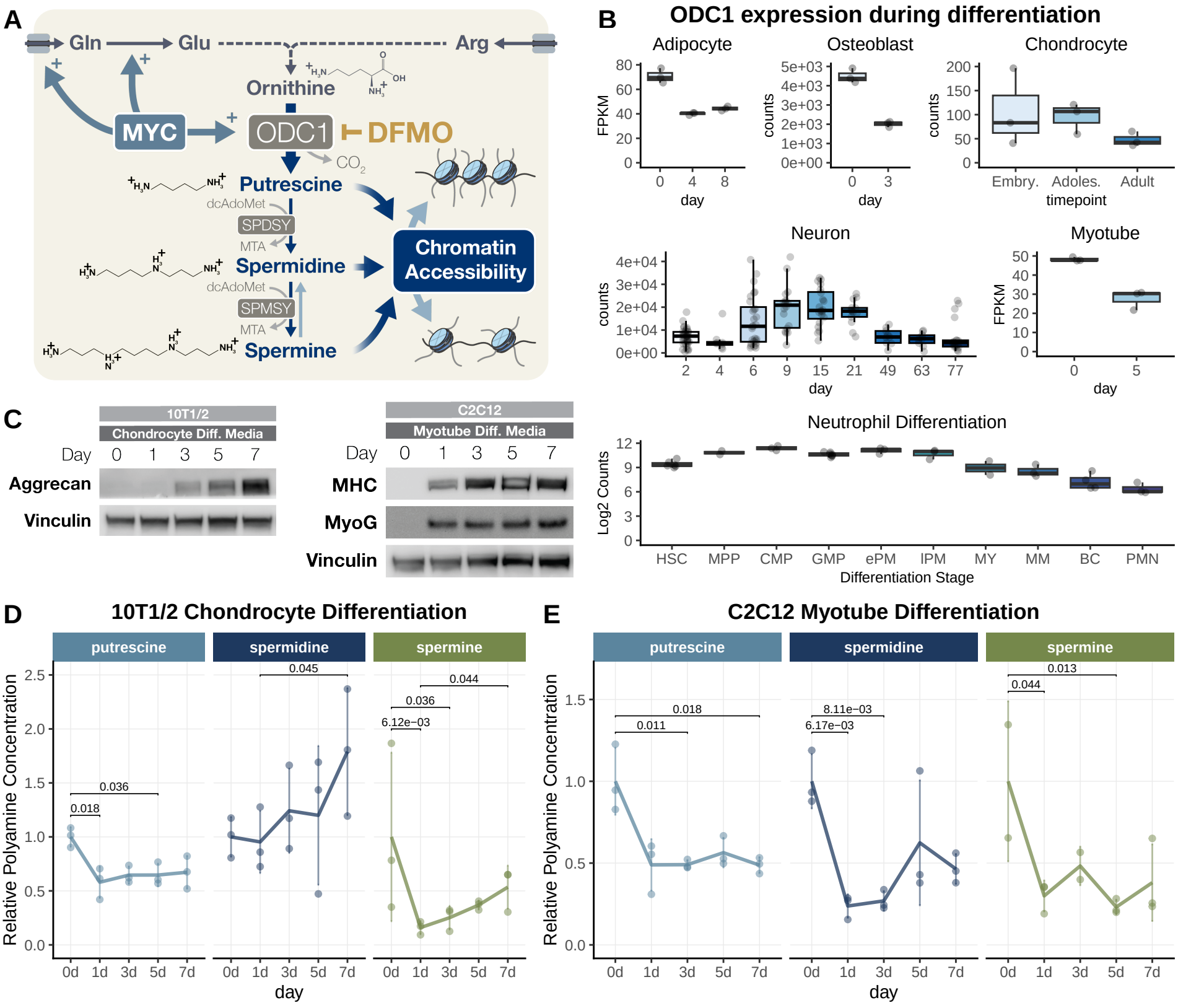
A
Gln
Glu
Arg
Ornithine
MYC
ODC1
DFMO
CO2
Putrescine
dcAdoMet
SPDSY
MTA
Spermidine
dcAdoMet
SPMSY
MTA
Spermine
Chromatin Accessibility
B
ODC1 expression during differentiation
Adipocyte
FPKM
day
Osteoblast
counts
day
Chondrocyte
counts
Embry.
Adoles.
Adult
timepoint
Neuron
counts
day
Myotube
FPKM
day
Neutrophil Differentiation
Log2 Counts
HSC
MPP
CMP
GMP
ePM
lPM
MY
MM
BC
PMN
Differentiation Stage
C
10T1/2
Chondrocyte Diff. Media
Day
Aggrecan
Vinculin
C2C12
Myotube Diff. Media
MHC
MyoG
Vinculin
D
10T1/2 Chondrocyte Differentiation
putrescine
spermidine
spermine
Relative Polyamine Concentration
0.036
0.018
0.045
0.044
0.036
6.12e−03
day
E
C2C12 Myotube Differentiation
putrescine
spermidine
spermine
Relative Polyamine Concentration
0.018
0.011
8.11e−03
6.17e−03
0.013
0.044
day

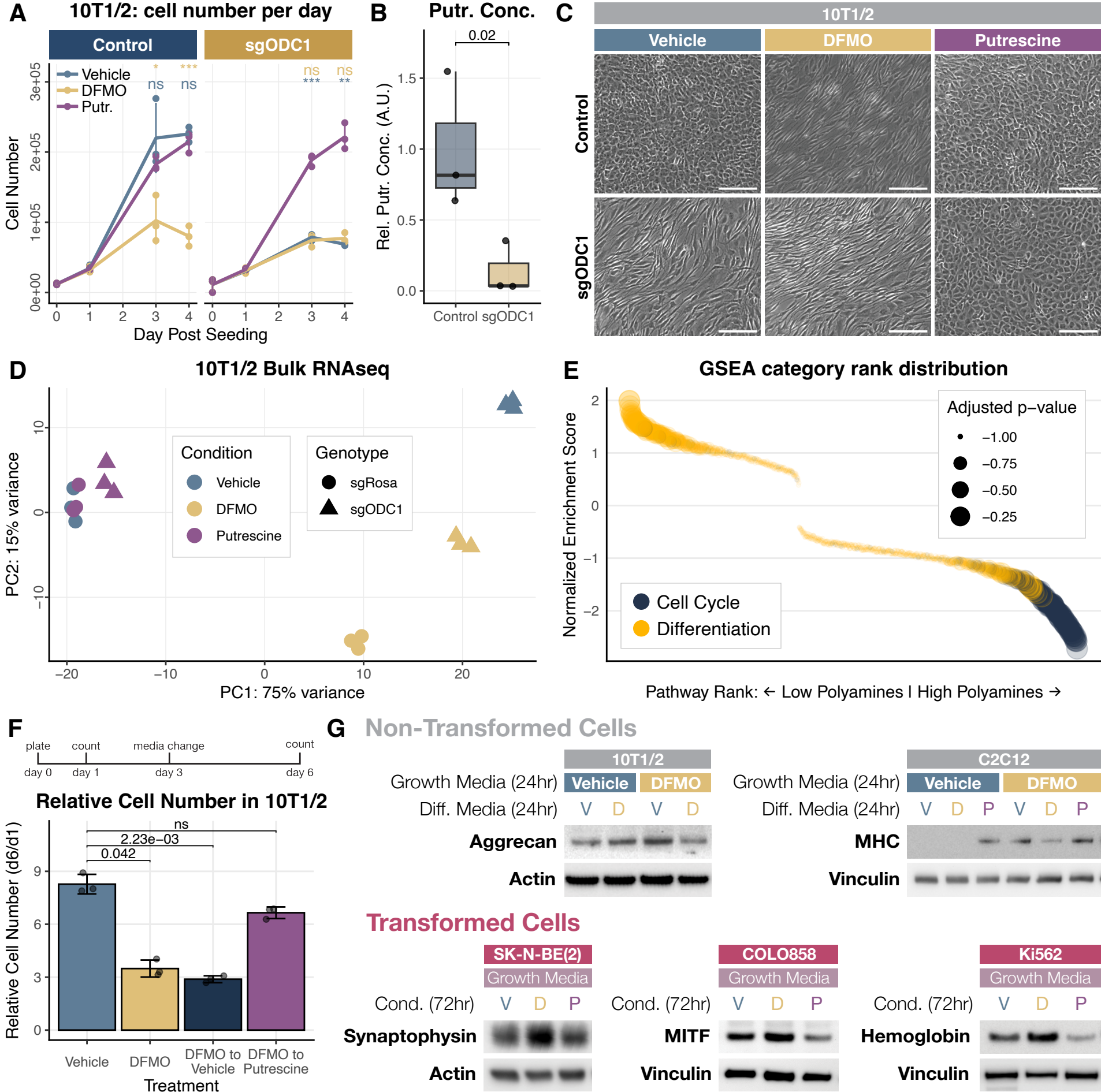
A
10T1/2: cell number per day
Control
sgODC1
Vehicle
DFMO
Putr.
Cell Number
Day Post Seeding
B
Putr. Conc.
0.02
Rel. Putr. Conc. (A.U.)
Control sgODC1
C
10T1/2
Vehicle
DFMO
Putrescine
Control
sgODC1
D
10T1/2 Bulk RNAseq
Condition
Vehicle
DFMO
Putrescine
Genotype
sgRosa
sgODC1
PC2: 15% variance
PC1: 75% variance
E
GSEA category rank distribution
Adjusted p−value
−1.00
−0.75
−0.50
−0.25
Normalized Enrichment Score
Cell Cycle
Differentiation
Pathway Rank: ← Low Polyamines | High Polyamines →
F
plate
count
media change
count
day 0
day 1
day 3
day 6
Relative Cell Number in 10T1/2
ns
2.23e−03
0.042
Relative Cell Number (d6/d1)
Vehicle
DFMO
DFMO to Vehicle
DFMO to Putrescine
Treatment
G
Non-Transformed Cells
10T1/2
Growth Media (24hr)
Vehicle
DFMO
Diff. Media (24hr)
V D V D
Aggrecan
Actin
C2C12
Growth Media (24hr)
Vehicle
DFMO
Diff. Media (24hr)
V D P V D P
MHC
Vinculin
Transformed Cells
SK-N-BE(2)
Growth Media
Cond. (72hr)
V D P
Synaptophysin
Actin
COLO858
Growth Media
Cond. (72hr)
V D P
MITF
Vinculin
Ki562
Growth Media
Cond. (72hr)
V D P
Hemoglobin
Vinculin

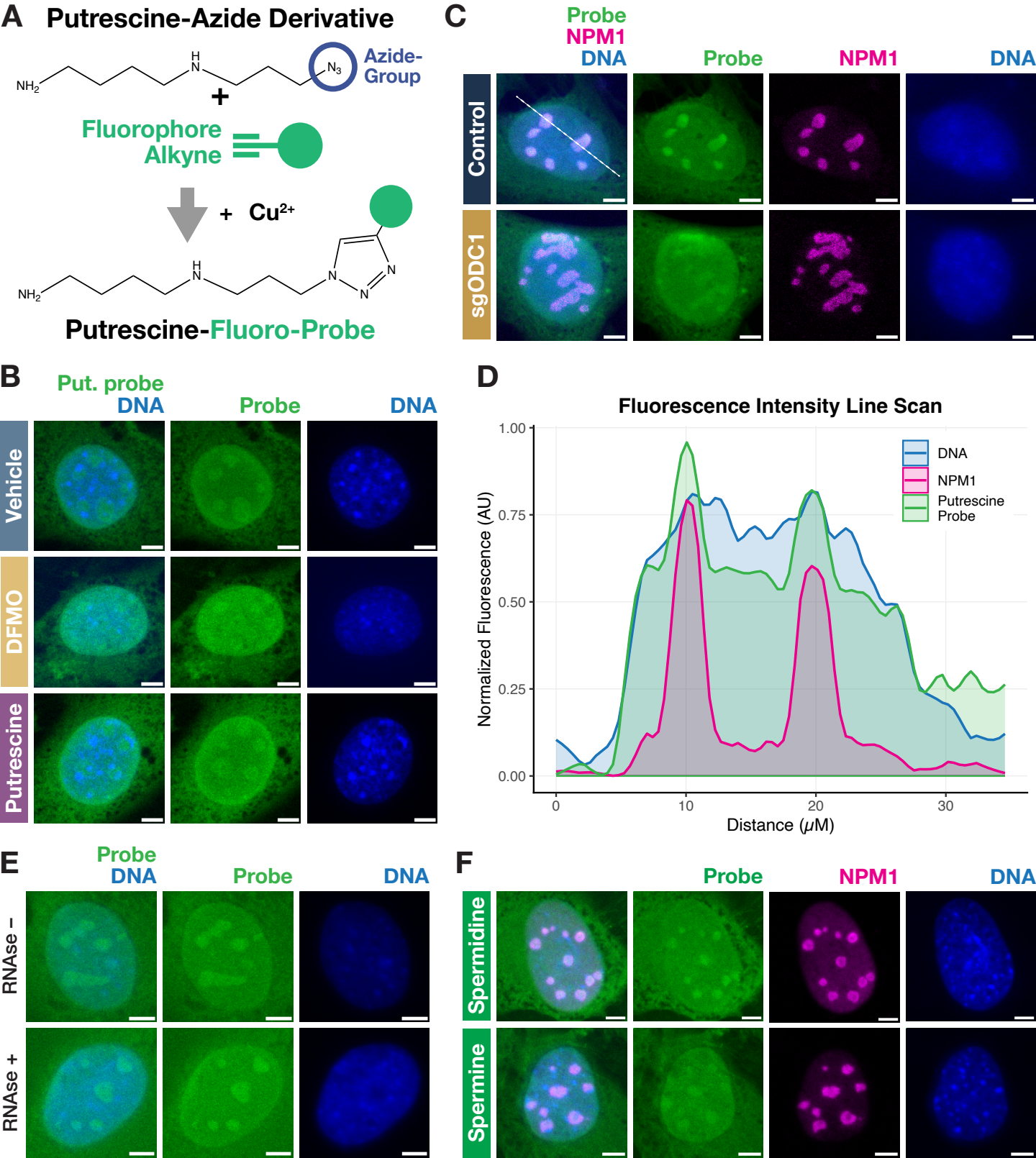
A
Putrescine-Azide Derivative
Azide-Group
Fluorophore Alkyne
+ Cu2+
Putrescine-Fluoro-Probe
B
Put. probe
DNA
Probe
DNA
Vehicle
DFMO
Putrescine
C
Probe
NPM1
DNA
Probe
NPM1
DNA
Control
sgODC1
D
Fluorescence Intensity Line Scan
Normalized Fluorescence (AU)
Distance (μM)
DNA
NPM1
Putrescine Probe
E
Probe
DNA
Probe
DNA
RNAse −
RNAse +
F
Probe
NPM1
DNA
Spermidine
Spermine

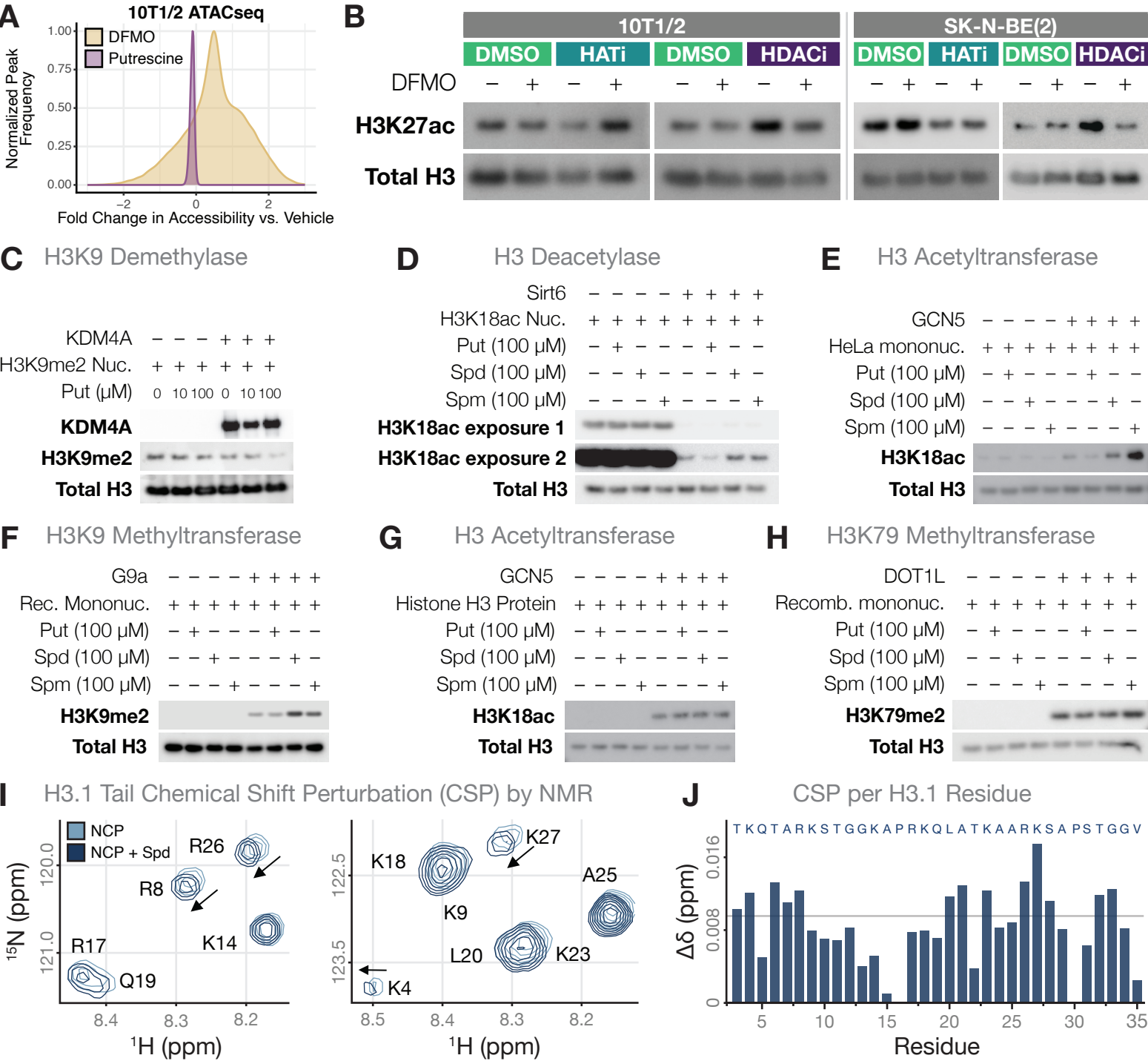
A
10T1/2 ATACseq
DFMO
Putrescine
Normalized Peak Frequency
1.00
0.75
0.50
0.25
0.00
−2
0
2
Fold Change in Accessibility vs. Vehicle
B
10T1/2
SK-N-BE(2)
DMSO
HATi
DMSO
HDACi
DMSO
HATi
DMSO
HDACi
DFMO
H3K27ac
Total H3
C
H3K9 Demethylase
KDM4A
H3K9me2 Nuc.
Put (μM)
0 10 100 0 10 100
KDM4A
H3K9me2
Total H3
D
H3 Deacetylase
Sirt6
H3K18ac Nuc.
Put (100 μM)
Spd (100 μM)
Spm (100 μM)
H3K18ac exposure 1
H3K18ac exposure 2
Total H3
E
H3 Acetyltransferase
GCN5
HeLa mononuc.
Put (100 μM)
Spd (100 μM)
Spm (100 μM)
H3K18ac
Total H3
F
H3K9 Methyltransferase
G9a
Rec. Mononuc.
Put (100 μM)
Spd (100 μM)
Spm (100 μM)
H3K9me2
Total H3
G
H3 Acetyltransferase
GCN5
Histone H3 Protein
Put (100 μM)
Spd (100 μM)
Spm (100 μM)
H3K18ac
Total H3
H
H3K79 Methyltransferase
DOT1L
Recomb. mononuc.
Put (100 μM)
Spd (100 μM)
Spm (100 μM)
H3K79me2
Total H3
I
H3.1 Tail Chemical Shift Perturbation (CSP) by NMR
NCP
NCP + Spd
R26
R8
R17
K14
Q19
K18
K27
A25
K9
L20
K23
K4
15N (ppm)
1H (ppm)
J
CSP per H3.1 Residue
T K Q T A R K S T G G K A P R K Q L A T K A A R K S A P S T G G V
Δδ (ppm)
Residue

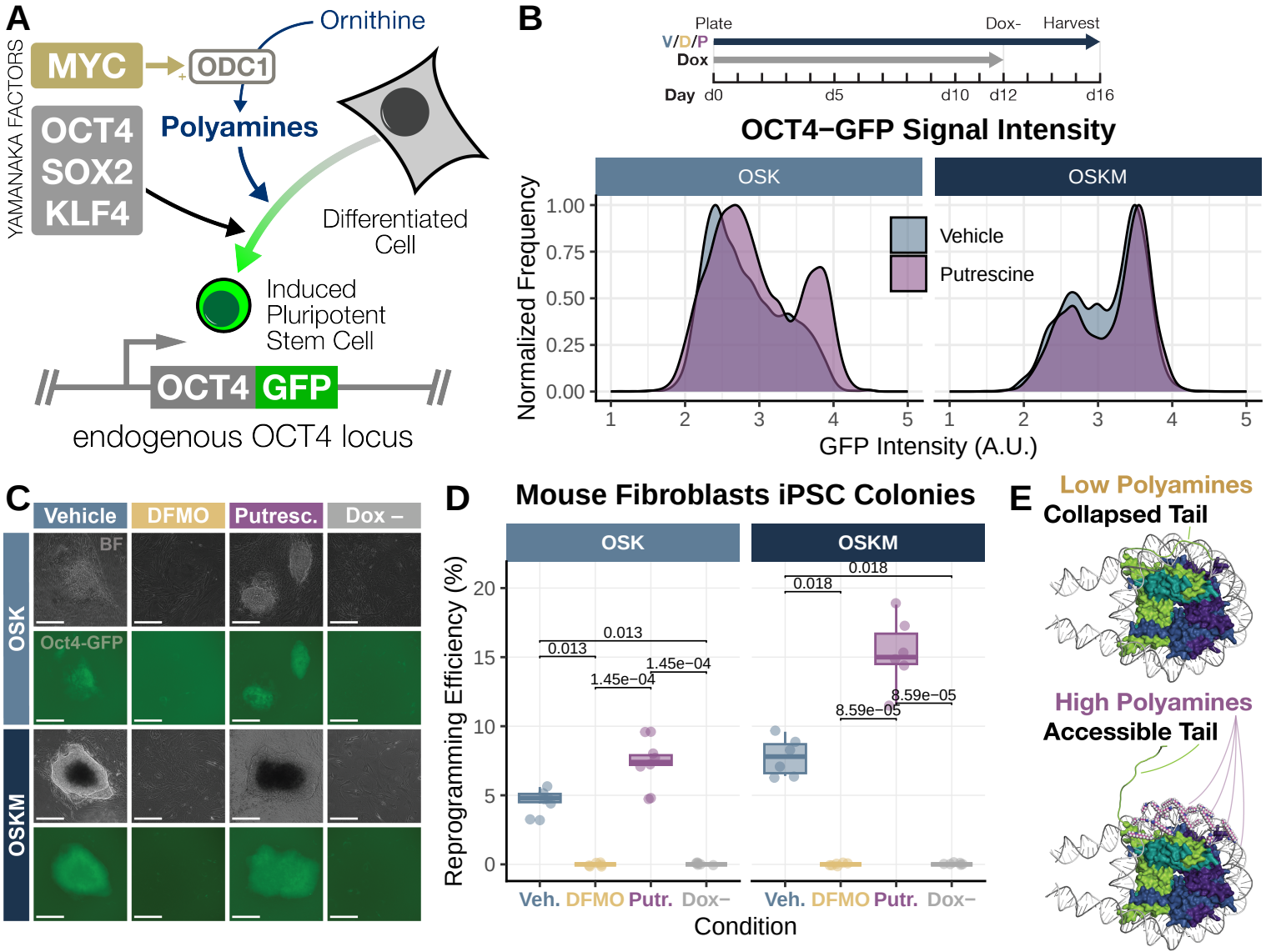
A
YAMANAKA FACTORS
MYC
ODC1
Ornithine
OCT4
SOX2
KLF4
Polyamines
Differentiated Cell
Induced Pluripotent Stem Cell
OCT4
GFP
endogenous OCT4 locus
B
Plate
Dox-
Harvest
V/D/P
Dox
Day d0 d5 d10 d12 d16
OCT4−GFP Signal Intensity
OSK
OSKM
Vehicle
Putrescine
Normalized Frequency
GFP Intensity (A.U.)
C
Vehicle
DFMO
Putresc.
Dox −
BF
Oct4-GFP
OSK
OSKM
D
Mouse Fibroblasts iPSC Colonies
OSK
OSKM
Reprogramming Efficiency (%)
0.013
1.45e−04
0.018
8.59e−05
Veh. DFMO Putr. Dox−
Condition
E
Low Polyamines
Collapsed Tail
High Polyamines
Accessible Tail